Saccharomyces cerevisiae CellWall Remodeling in the Absence of Knr4 and Kre6 Revealed by Nano-FourierTransform Infrared Spectroscopy

Gorkem Bakir, Tanya E S Dahms, Hélène Martin-Yken, Hans A Bechtel,
Kathleen M Gough

HAL Id: hal-04472218
https://hal.inrae.fr/hal-04472218v1

Submitted on 22 Feb 2024

Saccharomyces cerevisiae CellWall Remodeling in the Absence of Knr4 and Kre6 Revealed by Nano-FourierTransform Infrared Spectroscopy

Gorkem Bakir[1], Tanya E. S. Dahms[2], Helene Martin-Yken[3,4], Hans A. Bechtel[5], and Kathleen M. Gough[1] (iD)

Abstract

The cell wall integrity (CWI) signaling pathway regulates yeast cell wall biosynthesis, cell division, and responses to external stress. The cell wall, comprised of a dense network of chitin, β-1,3- and β-1,6- glucans, and mannoproteins, is very thin, <100 nm. Alterations in cell wall composition may activate the CWI pathway. Saccharomyces cerevisiae, a model yeast, was used to study the role of individual wall components in altering the structure and biophysical properties of the yeast cell wall. Near-field Fourier transform infrared spectroscopy (nano-FT-IR) was used for the first direct, spectrochemical identification of cell wall composition in a background (wild-type) strain and two deletion mutants from the yeast knock-out collection: kre6Δ and knr4Δ. Killer toxin resistant 6 (Kre6) is an integral membrane protein required for biosynthesis of β-1,6-glucan, while Knr4 is a cell signaling protein involved in the control of cell wall biosynthesis, in particular, biosynthesis and deposition of chitin. Complementary spectral data were obtained with far-field (FF)-FT-IR, in transmission, and with attenuated total reflectance (ATR) spectromicroscopy with 3–10 μm wavelength-dependent spatial resolution. The FF-FT-IR spectra of cells and spectra of isolated cell wall components showed that components of the cell body dominated transmission spectra and were still evident in ATR spectra. In contrast, the nano-FT-IR at ~25 nm spatial resolution could be used to characterize the yeast wall chemical structure. Our results show that the β-1,6-glucan content is decreased in kre6Δ, while all glucan content is decreased in the knr4Δ cell wall. The latter may be thinner than in wild type, since not only are mannan and chitin detectable by nano-FT-IR, but also lipid membranes and protein, indicative of cell interior.

Introduction

Saccharomyces cerevisiae, instrumental in brewing and baking, is a model organism for understanding yeast cell wall biology.[1] The S. cerevisiae cell wall is composed of inner and outer layers. The inner layer consists primarily of β-1,3-glucan chains with β-1,6 branches and β-1,6-glucan chains; chitin chains at the outer and inner surfaces of this layer confer significant tensile strength though they represent the smallest fraction (~2%) of the cell wall. The outer layer is predominantly comprised of a glycoprotein lattice (manno-protein).[2] The strength and elasticity of the yeast cell wall arise from these interwoven macromolecular components

[1]Department of Chemistry, University of Manitoba, Winnipeg, Manitoba, Canada
[2]Department of Chemistry and Biochemistry, University of Regina, Regina, Saskatchewan, Canada
[3]TBI, Université de Toulouse, CNRS, INRAE, INSA, Toulouse, France
[4]LAAS–CNRS, Université de Toulouse, Toulouse, France
[5]Advanced Light Source Division, Lawrence Berkeley National Lab, Berkeley, California, USA

Corresponding Author:
Kathleen M. Gough. Department of Chemistry, University of Manitoba, Winnipeg, Manitoba R3T 2N2, Canada.
Email: kmgough@cc.umanitoba.ca

which protect the organism from osmotic shock and mechanical stress while maintaining cell shape and enabling cell cycle progression and adhesion.[2–4] The chemical composition of the cell wall is difficult to determine by direct measurement, as it is on the order of 100 nm thick.[1,3]

The cell wall integrity (CWI) signaling pathway plays a critical role in the maintenance and remodeling of the cell wall, particularly during budding and in response to external stress.[5–7] In this study, we focus on deletion mutants of two *S. cerevisiae* proteins, killer toxin resistant 6 (Kre6) and Knr4, that are involved in cell wall biogenesis and have homologs across the fungal kingdom. Knr4 and Kre6 mutants were specifically chosen for investigation in this study due to their known roles in cell wall biogenesis and their presence across multiple fungal species, including pathogenic yeasts, indicating their potential significance and similarity in understanding cell wall-related processes.

Killer toxin resistant 6 (Kre6) is a type II integral membrane protein that plays a key role in the biosynthesis of β-1,6-glucan.[5,8,9] In *S. cerevisiae,* simultaneous deletion of Kre6 and its homolog Skn1 results in a severe growth defect.[10] In *Aureobasidium pullulans,* deletion of two Kre6-like homologs alters the cell wall and cell morphology, and reduces branching and overall production of soluble extracellular β-glucans, without clearly impacting cell viability.[11] The *Candida albicans* mutant *kre6Δ/Δskn1Δ/Δ* exhibits cell wall abnormalities and greatly diminishes cell growth.[12] Knr4 is a cell signaling protein involved in the control of cell wall biosynthesis and cell cycle, as well as chitin deposition during vegetative growth and sporulation.[13–16] In the human fungal pathogen *C. albicans,* Knr4 has two homologs, Smi1 and Smi1B, that are involved in adhesion and antibiotic resistance.[17,18] These observations show that Kre6, Knr4, and their homologs have conserved roles in cell wall biogenesis among these fungi.

In the studies of Kre6[8–12] and Knr4[13–18] above, yeasts and wall composition were investigated by conventional fluorescence staining of cells or by extraction and isolation of components for chemical analysis. Infrared (IR) spectroscopy has been used to gain insight into cellular composition based on known IR absorption bands, many of which are distinct for various biocomponents: proteins, fats, and sugars, including chitin and glucans.[19–22] Building on our recent study of *Aspergillus* fungal cell walls,[19] we have now used far-field (FF) and near-field nanoscale (nano)-FT-IR spectroscopy on intact yeast cells to explore differences in the cell wall composition of a wild-type (wt) strain and two yeast knock-out (YKO) strains: *kre6Δ* and *knr4Δ*. FF-FT-IR hyperspectral images were recorded from whole cells in transmission mode and by attenuated total reflection (ATR) with a microdevice (FF-FT-IR + ATR), with an FT-IR microscope and a focal plane array (FPA) detector. Although the ATR spectra should contain a relatively greater contribution from the cell wall than transmission spectra, both methods probe whole cells at the μm scale. These FF spectra served as a basis for comparison with nano-Fourier transform IR spectroscopy (nano-FT-IR) spectra recorded with scattering scanning near-field optical microscopy (s-SNOM), which should access only the cell wall, by probing a voxel on the order of ~25 nm.[23–27] Herein, we present the first direct nanoscale spectrochemical analysis of differences in the cell walls of these wt and mutant strains.

Materials and Methods

Wild-type (wt; BY4741), *knr4Δ*, and *kre6Δ* strains of *S. cerevisiae* were obtained from the Open Biosystems YKO collection. Yeast extract peptone dextrose broth (YPD, Y1375) and bacteriological agar (A5306) were purchased from Sigma-Aldrich. Ultra-pure (18 MΩ) water was obtained by filtration (Thermo Scientific Barnstead Easypure II system). Reference standards of isolated components, i.e., chitin (C9752), laminarin (L9634), mannan (M7504), and β-1,3-glucan (89862), were purchased as powders from Sigma-Aldrich Co. IR transparent BaF_2 crystal windows (25 mm diameter, 2 mm thick, COE Optics) were used for FF-IR transmission spectroscopy. Gold-coated silicon wafers (AuSi) were prepared in-house and cut into ~1 cm squares for FF micro-ATR and nano-FT-IR of yeast cell walls.

Yeast Cell Preparation

Yeast cells were cultured for 24 h at 30 °C on a YPD solid medium (50 g/L YPD broth, 20 g/L agar) in Petri dishes. For each strain, a single mature colony was removed from the culture plate, suspended in 1 mL of ultra-pure water, and centrifuged for 5 min at 5300 *g*; the supernatant was discarded. This procedure was repeated three times, then cells were resuspended in 1 mL of ultra-pure water. A 5 μL aliquot from this suspension was placed onto either an AuSi square or a BaF_2 window, dried in a desiccator at room temperature for 15–30 min, and stored in a sealed plastic case, in the dark, at room temperature until IR data collection.

FF-FT-IR Transmission and ATR

Cells on BaF_2 windows were imaged in transmission mode with an Agilent Cary 670 interferometer and a 620 IR microscope equipped with an FPA mercury cadmium telluride (MCT) detector with normal magnification optics (15×, 0.62 NA), yielding a 64 × 64 array of 4096 spectra with an effective geometric pixel size of 5.5 × 5.5 μm². Sample spectra were acquired as 128 co-added scans (6 min) using ResolutionsPro software (version 5.3.01964, Agilent Technologies Inc.). Sample spectra were normalized against a background of 256 scans taken on a clean area of the BaF_2 window.

The FF-FT-IR + ATR spectra were acquired from yeast cells on AuSi squares with the Agilent slide-on micro-ATR accessory (Ge crystal), as sums of 128 sample scans ratioed against an air background of 512 scans. All spectra were collected at 4 cm^{-1} spectral resolution. The index of refraction

of Ge is 4, thus the effective geometric pixel size is 1.4×1.4 μm^2 in the ATR–FPA image, with a wavelength-dependent penetration depth of about 1 to 1.5 μm. ATR spectra were corrected for the wavelength dependence of penetration depth into the sample using ResolutionsPro software. FF-FT-IR + ATR spectra of standard carbohydrates in powder form were collected with a Bruker Alpha-P FT-IR spectrometer (diamond crystal) as sums of 128 sample scans ratioed against an air background of 512 scans; the ATR correction was applied automatically in the Bruker OPUS software (version 7.2.139.1294).

Atomic Force Microscopy Imaging and Near-Field Nano-FT-IR

The AFM images were recorded with a specially modified AFM (Innova, Bruker) within the synchrotron IR nanospectroscopy (SINS) instrument[23] on beamline 5.4 at the Advanced Light Source (ALS), Lawrence Berkeley National Laboratory. AFM images were collected in tapping mode using a platinum silicide AFM tip (Nanosensors PtSi-NCH), for which the cantilever had a nominal resonant frequency of 330 kHz. The radius of these tips is <25 nm and we typically resolve features of <20 nm in test images. AFM images were processed with the Gwyddion imaging software (version 2.51, Brno).[24] Isolated single yeast cells were identified by AFM prior to nano-FT-IR. Cells with heights <2.5 μm were selected for analysis since they were within the AFM z-piezo range.

The SINS system is constructed as an asymmetric Michelson interferometer.[23] Synchrotron IR light is passed through a

beamsplitter such that half of the light illuminates the AFM tip while the other half is directed to the moving mirror of a modified commercial rapid scan FT-IR spectrometer (Nicolet 6700, Thermo Scientific). The backscattered light from the tip is combined with the reflected light from the reference moving mirror and interferometrically detected with an MCT detector.

A background spectrum was first recorded on a clean portion of the AuSi square. An AFM scan of the target cell was used to locate a suitable region for spectral acquisition. For each background and sample spectrum, 512 scans were co-added with a spectral resolution of 8 cm^{-1}. A rapid AFM scan, typically 2×2 μm^2, with 20 nm step size, was recorded immediately prior to and after each spectral acquisition to ensure that the target cell had not drifted. Typically, three or four sample spectra were acquired, followed by a collection of a new background spectrum to allow for slight variations in beam alignment. The total time to acquire a spectrum was typically about 15 min, given 6 min per spectrum, the requirement for frequent background spectra, and numerous rapid AFM images to counter drift.

For all near-field spectra, the second-order scattering amplitude $s_2(\omega)$ and phase $\varphi_2(\omega)$ spectra were obtained by demodulating the interferometric signal at the second harmonic of the tip tapping frequency with a lock-in amplifier and then Fourier transforming the resulting signal using a custom Fourier transform analysis package (Nanospectroscopy Data Analysis, version 2, ALS). Nano-FT-IR spectra of yeast were normalized against background spectra acquired at a clear surface on the AuSi square, according to Eq. 1:

$$\text{Nano-FT-IR spectrum} = \frac{s_2(\text{yeast}, \omega)}{s_2(\text{gold}, \omega)} \sin[\varphi_2(\text{yeast}, \omega) - \varphi_2(\text{gold}, \omega)] \tag{1}$$

For our data, tapping amplitudes of ~70–90 nm were used, as per the recommended settings for optimal signal.[27] Spectral bands from the known tip contaminant, polydimethylsiloxane (PDMS),[27] were removed by subtracting a reference PDMS spectrum from any sample spectrum in which it appeared.

Results

Infrared (IR) spectra from all three methods were used to characterize the cell wall composition and to compare differences among the three *S. cerevisiae* strains (wt BY4741, *knr4Δ*, and *kre6Δ*). Each method provided a different perspective: whole cell (FF-FT-IR), cell wall plus some cytoplasm (FF-FT-IR + ATR), and cell wall alone (nano-FT-IR). Initial analyses were based on the presence and relative intensity of standard reference absorption bands for protein (amide I at ~1650 cm^{-1}, mainly carbonyl stretch mode, and amide II at 1545 cm^{-1}, mainly protein C–N stretching + N–H bending)

and bands in the predominantly carbohydrate region (900–1200 cm^{-1}).[19,22,28–30]

FF-FT-IR Transmission Spectroscopy of Yeast Cells

For each strain, several FPA hyperspectral images were collected from freshly harvested cells mounted on BaF_2 windows (Figure 1). Typical bright-field images (Figure 1, left column) showed numerous dense yeast cell clusters, in which the cells appeared dark against the transparent salt window. False-color FPA images were generated in ResolutionsPro by integrating the area of the amide I band (Figure 1, middle column) showed that IR absorption by protein corresponded to the cell locations, as expected. The wavelength-dependent spatial resolution at 1650 cm^{-1} is ~6 μm; therefore, with the FF optical setup, individual cells within a cluster could not be resolved. Since cells had a rounded shape with dimensions on the order of the IR
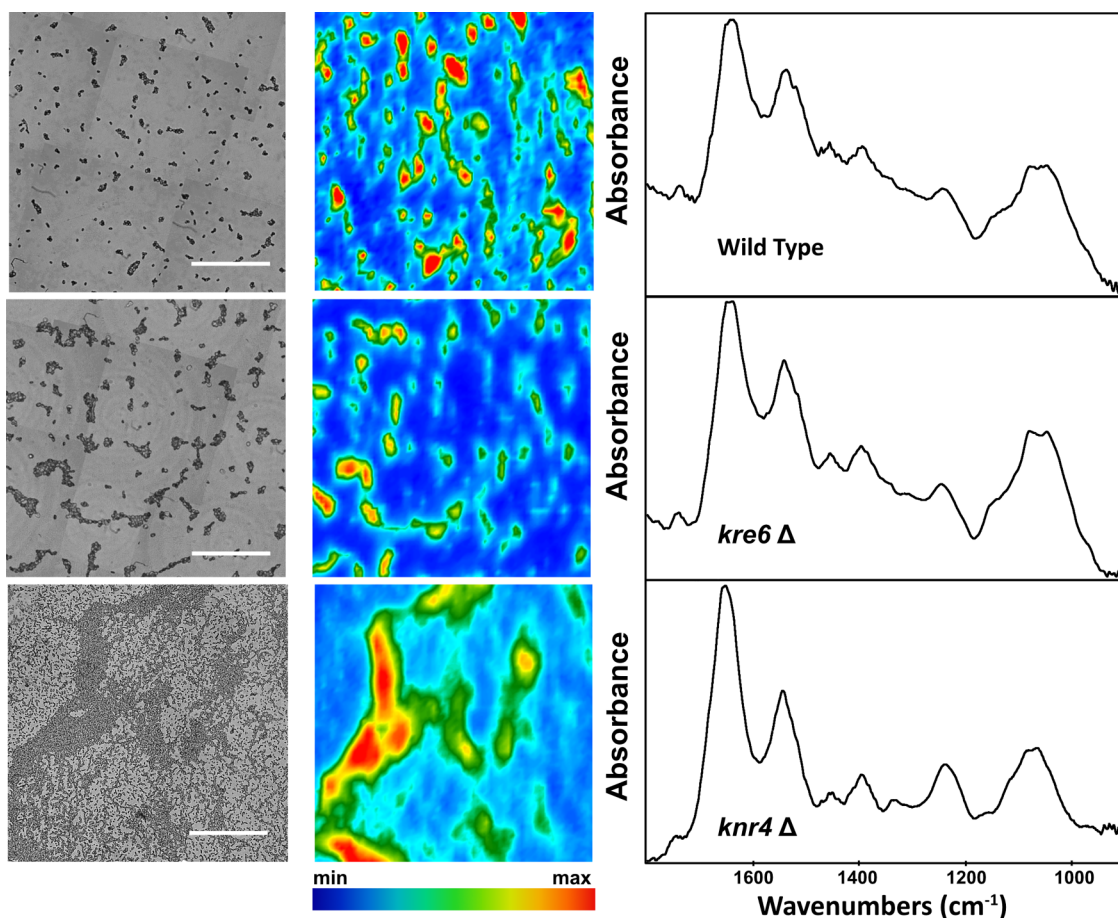
Figure 1. Images of wt BY4741, *kre6Δ*, and *knr4Δ* whole cells recorded in bright-field and transmission FF-FT-IR with FPA. (Left) Bright-field images of cells mounted on BaF_2 windows. Scale bar = 100 μm. (Center) Corresponding false-color 64 × 64 FPA images, processed on the integrated area of the amide I band at 1650 cm^{-1}. Maximum signal (red) corresponds to the location of cells and cell clusters. (Right) Average of 20 best-quality spectra extracted from each image.

wavelengths, some spectra exhibited significant Mie and Resonant Mie scattering (RMieS) artifacts, including rolling baselines and dispersion-like characteristics in strong bands.[31–33] Average spectra were created from the 20 best spectra from each image, selected for the best signal-to-noise ratio (S/N), baseline flatness, and absence of scattering artifacts (Figure 1, right column). All spectra contained traces of water vapor that were removed by subtracting a spectrum from within the same FPA image where cells were absent (see Figure S1, Supplemental Material). In the average spectra of all 3 strains, the bands for the amide I and II modes were much stronger than those in the predominantly carbohydrate region (900–1200 cm^{-1}). Despite some observable differences among the strains, bands from the cell body, such as C = O from lipid membranes at 1740 cm^{-1} were strongly evident. It was concluded that the FF-FT-IR transmission spectra of cells on salt windows represented the content of the whole cell body, as had been anticipated. As such, the FF-FT-IR transmission spectra provided a useful whole cell standard for comparison with ATR and nano-FT-IR data.

Spectral and structural differences were explored further with IR methods that probe smaller voxels, to approach spectra that reflect primarily the cell wall composition.

FF-FT-IR + ATR of Wild Type and Mutants

The FF-FT-IR + ATR spectra of the three yeast strains were collected by direct crystal contact with cells mounted on AuSi squares, at several locations for each strain (Figure 2). The micro-ATR field of view was focused onto the FPA, again yielding an array of 64 × 64 spectra at each contact site. Bright-field microscopy images (Figure 2, insert) show the cells before and after the ATR crystal touchdown. In each case, a cluster of cells had been disturbed, evidence that they had been contacted directly. Yeast cells are sharply rounded and hard, resulting in poor contact with the ATR crystal (Figure S2, Supplemental Material). The spectra in Figure S2 (Supplemental Material) were created by averaging the 20 best spectra from FPA images for each strain, with selection based on the same criteria adopted for the
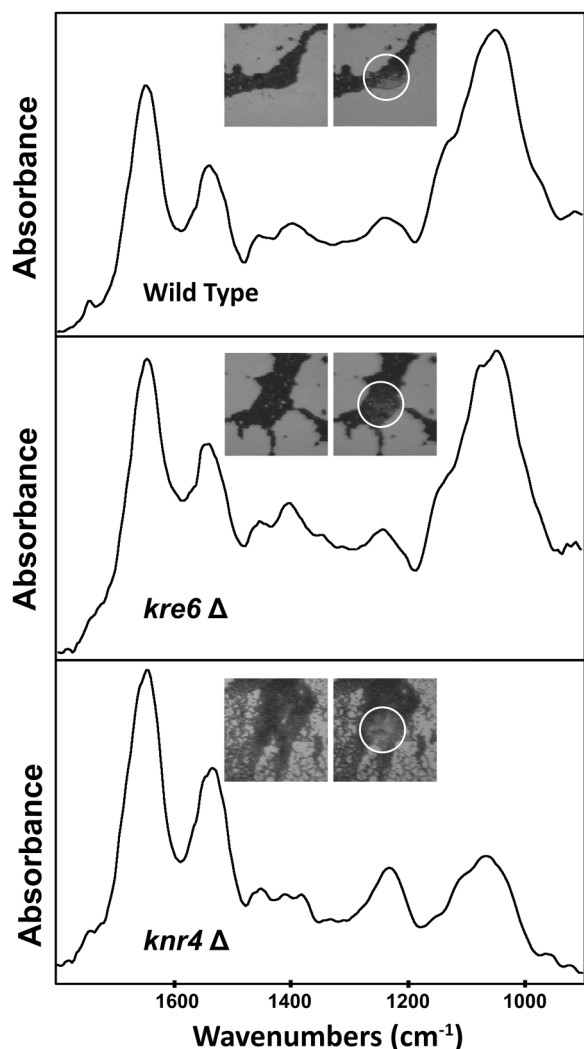
Figure 2. Bright-field images (insets) and FF-FT-IR – ATR spectra of wt, *kre6*Δ, and *knr4*Δ whole cells mounted on AuSi squares. Spectra are an average of the best 20 spectra from the FPA image. Bright-field 15× images, before (left) and after (right) ATR crystal touch down, show the contact region for each.

transmission FF-FT-IR. The original ATR spectra (Figure 3, Supplemental Material) contained water vapor bands and required the standard ATR correction for wavelength-dependent depth penetration. After the removal of water, the standard ATR correction was applied in the ResolutionsPro software using the refractive index of 4.003 for Ge, and 1.5 for the yeast cells. The relative intensity of the carbohydrate bands had increased noticeably relative to that of amide bands, as seen in the whole cell spectra acquired in transmission mode, but the lipid C=O band was still evident.

Nano-FT-IR of Yeast Strains

For the Nano-FT-IR, replicate spectra were recorded from three wt cells, nine *kre6* mutant cells, and 10 *knr4* mutant cells. Representative topographic AFM images of three

individual yeast cells, one from each strain, are shown in the left column of Figure 3; circles indicate where spectra were taken (15 spectra each for wt and *knr4*Δ, 22 spectra for *kre6*Δ). The total broadband scatter images (Figure 3, middle column) showed lower IR scatter across each cell; hence, they appear to be very dark. Scattering was high in the bright non-absorbing surrounding regions. We noted interesting patterns in the IR scattering images, particularly the bright spots around the cell locations. These are artifacts due to the illumination geometry and the curvature and dimension of the cells, which caused the cells to act as nano lenses for the incident IR light.

Nano-Fourier transform infrared spectroscopy (nano-FT-IR) spectra (Figure 3, right column) were created by averaging single-point spectra for each cell to improve the S/N. Band intensities in the carbohydrate region were much more prominent in wt and *kre6*Δ compared to the amide bands, evidence that only the carbohydrate-rich cell wall was probed by nano-FT-IR.[34]

Band assignments for the target compounds are summarized in Table I, based on data recorded here and in other yeast cell studies. Two references noted traces of protein, 2–6%, in the isolated carbohydrate samples[28,30]; another used whole cell ATR which necessarily probed cell interior;[35] while others were recorded in media.[20,21] Despite the useful information provided, the presence of other materials impeded clear assignments. Therefore, ATR spectra of isolated wall components were acquired as reference standards (Figure 4) to corroborate band positions reported in the literature and to enable direct comparison with our nano-FT-IR spectra. A weak band at 1645 cm^{-1} in the spectra of mannan and the glucans was evident in literature spectra;[30] those samples were reported as having water content of up to 10.8% by mass. The same band was observed here (Figure 4) and was assigned as the bending mode of residual water. Given the preponderance of OH bonds in carbohydrates, it was not possible to assess water from the OH stretch region of the reference spectra, nor was it useful as the near-field IR spectra did not extend to this region.

Discussion

Wild-type (wt) and mutant *S. cerevisiae* have often been used as important models for understanding the cell surface biology of yeasts. To this end, structure and composition have been studied with a wide variety of methods, many of which require chemical, mechanical, or enzymatic extraction and isolation of cell wall components for subsequent chemical analyses, electrophoresis, chromatography, fluorescence, nuclear magnetic resonance, etc.[8,10,36–38] The goal of the present study was to image wt and cell wall biogenesis mutants by IR spectroscopic methods from the μm to nm scale, in order to interpret cell wall spectral signatures, detected in situ, in the context of changes in macromolecular composition.

Kre6 and Knr4 are proteins responsible for the biosynthesis of cell wall components, particularly for β-1,6-glucan and
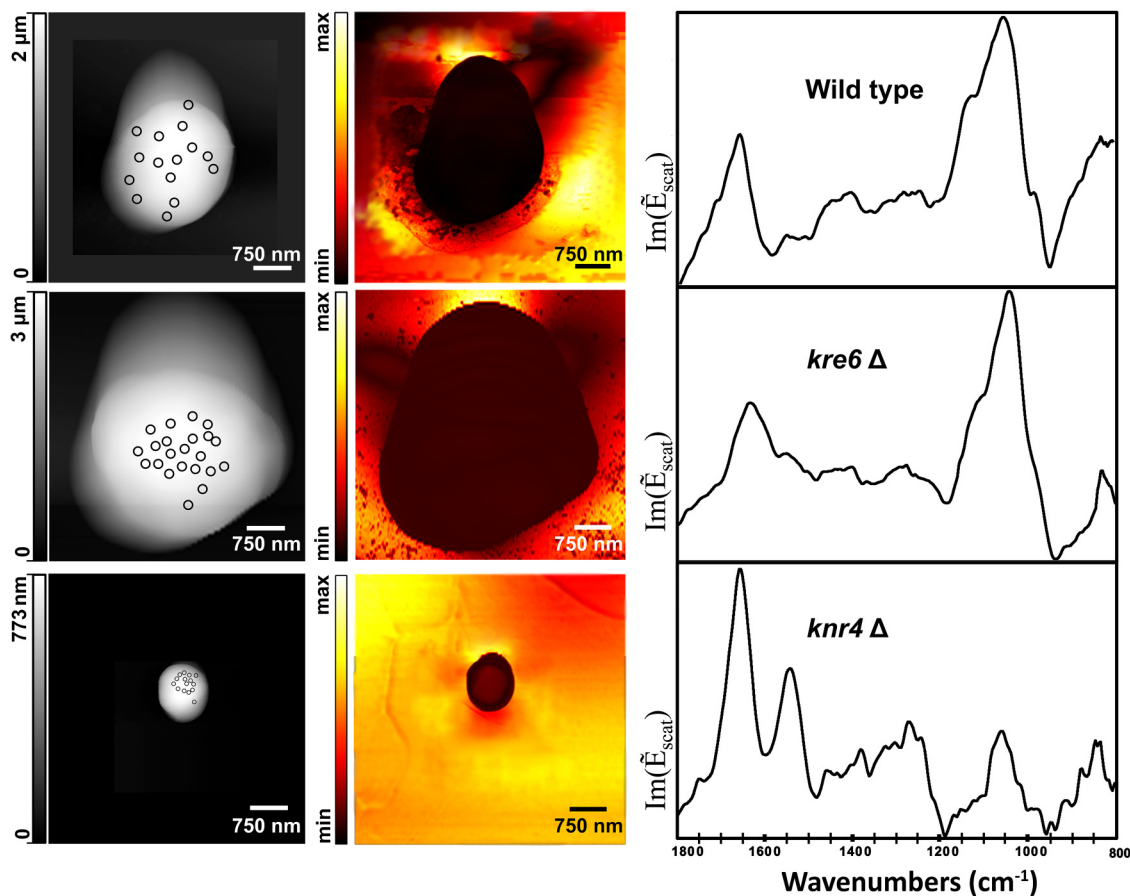
Figure 3. Atomic force microscopy (AFM) and nano-FT-IR images and spectra of cells mounted on AuSi squares, recorded in tapping mode. (Left) AFM topography images of individual cells; circles show where spectra were collected. (Center) nano-FT-IR heat map image, showing total broadband IR scattering. (Right) Nano-FT-IR spectra for each cell averaged from 15 spectra each for wt and *knr4Δ* and 22 spectra for *kre6Δ*.

Table I. Nano-FT-IR band positions (cm^{-1}) and assignments for *S. cerevisiae* strains.

Wild-type	*kre6Δ*	*knr4Δ*	Assignment	References[a]
803, 829, 859, 880, 900	811, 830, 882, 916, 976	815, 834, 844, 879, 911, 975	Mannan	20,21
988		992	β-1,6-glucans	20,21,35
1031	1042	1039	β-glucan	35
1119–1135	1112–1136	1111	ν (CC), C–O–C chitin, β-glucan	22,29
1150	1156	1151	C–O, C–OH, chitin, β-glucan	29
		1375, 1309	Chitin	This work (Figure 4)
1500–1190	1500–1190	1500–1190	carbohydrates	This work (Figure 4)
1548	1547	1542	Amide II	This work
1633	1634, 1612	1631	ν (C=O), chitin (acetamide)	22,29
1663	1634 (broad)	1656	amide I (C=O), chitin (acetamide)	22,28,30
		1748	Lipid carbonyl	This work

[a]All literature assignments were reconfirmed with our reference spectra (Figure 4).

β-1,3-glucan, respectively. Their absence enforces reliance on different pathways or linkages to build and maintain the cell wall.[8,13] The *S. cerevisiae* wt and *knr4Δ* strains have been studied using AFM and force spectroscopy to assess cell wall elasticity and its relationship to cell wall chemical composition as

determined by standard isolation and chromatography.[39] The authors found that cell wall elasticity was reduced by 50% in the *knr4Δ* strain in the stationary phase, along with increased surface roughness in the cell surface topology. Isolation of cell wall components showed that the relative amounts of
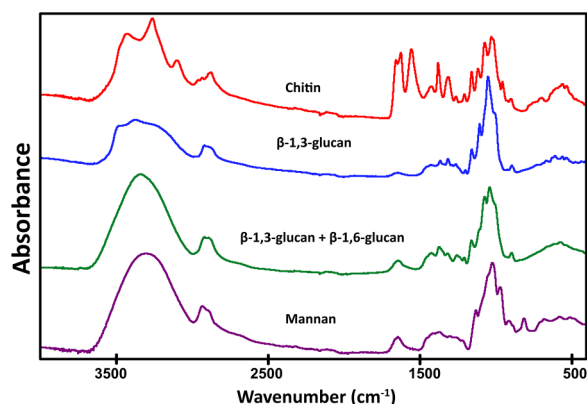
Figure 4. ATR spectra of isolated cell wall carbohydrate standards.

β-glucan, mannan, and chitin changed from 50%, 49%, and 1% to ~30%, 67%, and 3%, respectively. However, they could not correlate roughness or elasticity with cell wall composition for several different but similar mutants.

Roemer and Bussey[8] found reduced levels of both β-1,3- and β-1,6-glucan in isolates from the cell walls of *kre6Δ* strains. More recently, cell lysates from *kre6Δ* strains were investigated using Western blotting with enhanced chemiluminescence detection, and whole cells (fixed and stained) were imaged with immunofluorescence microscopy and immunoelectron microscopy.[9] A significant portion of Kre6 was found in the polarized plasma membrane buds required for β-1,6-glucan synthesis, though there was no direct chemical analysis of the cell wall composition. Han et al.[12] observed *C. albicans kre6Δ/Δ* cells grown in media, using bright-field and transmission electron microscopy, showing that the kre6 gene was not essential for the viability, but its double mutation resulted in cell separation defects when *SKN1* was suppressed.[12] None of the techniques noted above allow direct, non-disruptive chemical analysis of the cell wall. However, with label-free IR spectroscopic imaging of whole cells and cell wall components, direct chemical identification of cell wall composition can be achieved at the nanoscale level, without staining or cell wall isolation.[19]

The FF-FT-IR transmission mode imaging with normal magnification optics measures the chemical composition at voxel dimensions that are nominally $5 \times 5 \times 5$ μm^3. These voxels are subject to the Rayleigh diffraction limit, where the IR wavelengths range from 2.5 to 12 μm in our spectra.[40] Mie scattering artifacts in FF-FT-IR can further compromise spectral analysis of single cells, whether in transmission or transflection.[41–43] Here, spectra were collected from small clusters of cells to minimize such artifacts. The FF-FT-IR spectra in Figure 1, selected to be artifact-free, contain information from the cell wall, membranes, cytoplasm, and internal organelles. Numerous vibrational bands characteristic of cell content were observed, including those from fatty acid esters (C=O stretch, ~1740 cm^{-1}), proteins (amide I or C=O, ~1650 and amide II or N–H bend with C–N stretch, ~1545 cm^{-1}), phosphate groups in nucleic acids

and phospholipids (1300–1000 cm^{-1}), and carbohydrates (900–1200 cm^{-1}). In yeasts, amide I and II bands can also arise from the *N*-acetyl functional groups of chitin within the cell wall.

In the FF-FT-IR transmission spectra of all strains, the amide peak intensities were much higher relative to the bands in the carbohydrate region (Figure 1, right column). The 1740 cm^{-1} band assigned to lipid membrane bilayers was also clearly evident. Given that membranes and the majority of proteins are located in the cell interior, we conclude that the spectra are, not surprisingly, dominated by total cell content at this voxel dimension. The FF-FT-IR spectra provided a useful reference for whole cells and a reliable contrast for spectra acquired with methods that would provide better spatial resolution.[43]

Significant differences could be noted between transmission and ATR FF-FT-IR spectra for the wt and *kre6Δ* spectra, the most obvious being an increase in the relative intensity of carbohydrate to amide bands in the ATR spectra (Figure 2). This result is consistent with the cell dimensions (1–5 μm diameter).[15] With a probe depth of ~1.4 μm, the ATR spectra sample less of the cell interior and would therefore contain proportionally more information on the carbohydrate-rich cell walls. Spectral differences within the carbohydrate regions of wt and *kre6Δ* included a shoulder emerging at ~990 cm^{-1}, assigned to β-1,6-glucan, and weak bands below 950 cm^{-1} that could be associated with the presence of mannan. The *knr4Δ* ATR spectra were very similar to those from whole cell transmission; this was ascribed to their smaller size, <2 μm, close to that of the ATR probe depth. For all strains, the carbonyl stretching mode from fatty acid esters (~1740 cm^{-1}) remained apparent. Despite the increased cell wall carbohydrate contribution to the wt and *kre6Δ* spectra, we concluded that the yeast cell interior was still evident, underscoring that neither the FF-FT-IR transmission nor ATR methods were sufficient to analyze changes in cell wall composition.

Given the nano-FT-IR probe depth of ~20–25 nm, SINS was anticipated to be ideal for directly probing the cell wall composition at the desired spatial resolution.[1,3,44] The s-SNOM technique yields wavelength-independent spectra and images without MieS or RMieS artifacts; however, the selection of data collection sites was still dependent on tip–sample interactions. The AFM images of wt and *kre6Δ* showed a strong edge effect,[39] attributed to their height and steeply curving sides. The *knr4Δ* cells were much smaller, with dimensions on the order of 750 nm to 1 μm, but still showed some edge effects. For all cells, good tip contact was maintained across the central upper surface as evidenced by the clear bright centers (Figure 3, AFM, left column) and dark scattering (Figure 3, total IR broadband scatter, middle column). Therefore, spectra were acquired only in this region of each cell. Spectral features were assigned and interpreted according to reference standards (Figure 4 and Table 1).

Wild-Type Nano-FT-IR Spectra. The carbonyl stretching mode from fatty acid esters (1740 cm^{-1}) was not apparent in the

wt nano-FT-IR spectrum (Figure 3, top right), evidence that signal arose only from cell wall components exterior to the cell's plasma membrane. Though a strong band with a maximum of ~1663 cm^{-1} was observed where the amide I is expected, the amide II band was much weaker. Therefore, bands in the 1500–1700 region were assigned as a combination of a small amount of protein (1656 and 1554 cm^{-1}) and water associated with the cell wall carbohydrates. Bands between 1500 and 1190 cm^{-1} were assigned to glucans and mannans. The shoulder at 988 cm^{-1}, assigned to β-1,6-glucan, was more obvious in the wt nano-FT-IR spectrum than in the FF ATR spectrum (Figure 2). The intensity of the carbohydrate region (glucans 1100–900 cm^{-1} and mannan peaks below 900 cm^{-1}) was increased relative to the amide + water bands compared to all FF spectra. Notably, the many prominent chitin peaks, i.e., 1654, 1622, 1375, and 1309 cm^{-1} (Figure 4, top) were not apparent in wt nano-FT-IR spectra, confirming that the volume probed did not extend to this innermost layer of the cell wall.

kre6Δ. The Kre6 protein localizes to the endoplasmic reticulum, plasma membrane, sites of polarized growth, and secretory vesicles.[8–10] Deletion of *KRE6* was reported to reduce the amount of β-1,6-glucan in the cell wall, as the gene product is directly responsible for the biosynthesis of β-1,6-glucan.[11,12] We have confirmed the effect of this mutation with the analysis of the *kre6Δ* nano-FT-IR spectra (Figure 3, middle, right). The band at 1740 cm^{-1} is not apparent and chitin bands are absent, again showing that only the outer cell wall had been probed. The ratio of band intensities for (amide + water) and carbohydrate bands was similar to that of wt spectra. The amide II band was still discernible despite the presumed presence of water, leading to a poorly resolved pair of band maxima at 1634 and 1552 cm^{-1}. Numerous overlapping bands in the 1500–1190 cm^{-1} region could be assigned as mixed carbohydrates (Table 1). The lower energy shoulder (~990 cm^{-1}) in the carbohydrate region assigned to β-1,6-glucan was not evident in the *kre6Δ* spectra. The intensity of mannan bands (at 975–800 cm^{-1}) in *kre6Δ* spectra were slightly reduced relative to those in the same region in the wt. Thus, the absence of specific bands and differences in the relative intensities are direct evidence that the β-1,6-glucan content is reduced in the *kre6Δ* wall.

knr4Δ. Knr4 is a cell signaling protein involved in the control of cell wall biosynthesis.[45] It is important for chitin deposition at bud sites and cell wall assembly and has been identified as a hub protein that interconnects numerous cell processes related to cell wall synthesis, cell cycle progression, and morphogenesis.[14] Kurita et al.[9] analyzed cell wall carbohydrate composition by acid hydrolysis of cells followed by anionic exchange chromatography to quantify the glucose, mannose, and chitin that were released.[39] They reported that the glucan/mannan ratio changes from 50:50 to about 30:65 in the *knr4Δ* mutant whether in stationary or exponential growth phase. Though still small, they found that the chitin content increases from ~0.6 to 1.2% in wt to 3.3 and 2.9% in the *knr4Δ* mutant, in exponential and stationary growth phases, respectively.

The profile observed in the nano-FT-IR spectrum of *knr4Δ* appeared to be significantly different from those of both wt and *kre6Δ*; however, we note that no statistical analysis was carried out. The lipid band at 1740 cm^{-1} was visible, suggesting that the plasma membrane was within the voxel. If so, then the cell wall was of the order of 30 nm thick, which could be consistent with the small cell size and the malformed cell state. The strong amide I band at ~1654 and weaker amide II at ~1550 cm^{-1} is more typical of protein than chitin, though the latter could easily be present in low amounts. Other chitin bands at 1375 and 1309 cm^{-1} were observed in the *knr4Δ* spectra, and with greater intensity than in the wt strain. The amide band intensities were much greater than the carbohydrate bands in *knr4Δ*, further evidence of contributions from the interior, although amide bands could also arise from mannoproteins located in the outermost layer of the cell wall.[38] The relatively weak intensity in the 1200–900 cm^{-1} region shows there is a significant reduction in β-1,3-glucan and β-1,6-glucan content. Unlike the wt and *kre6Δ*, the intensities of mannan bands in *knr4Δ* spectra are almost equal to the entire carbohydrate region (1200–900 cm^{-1}). Taken together, the nano-FT-IR spectra show that there is a significant reduction in glucans and a relatively greater amount of chitin and mannan in the *knr4Δ* wall than in either wt or *kre6Δ*.[13,14,39,45]

Conclusion

Mutations affecting the CWI pathway of *S. cerevisiae* result in altered cell wall structure and composition, but these changes are challenging to detect directly as the multi-component cell wall is only ~100 nm thick. By probing to ~1 μm depth, FF-FT-IR + ATR spectrochemical imaging provided a better window into the cell wall composition compared to that of FF-FT-IR in transmission mode. Despite the high quality of the spectral S/N, the wavelength-dependent spatial resolution limited further analysis in both FF methods. Through comparison of nano-FT-IR spectra from mutants and wt cells, we found that the β-1,6-glucan content is reduced in the cell wall of the *kre6Δ* mutant. Similar comparisons showed that the *knr4Δ* mutant had relatively less glucan overall, consistent with indirect evidence from previous studies. Depletion of glucans may have resulted in a much thinner cell wall in the *knr4Δ* mutant than in wt or *kre6Δ*, given our observation of chitin and mannan bands, as well as stronger lipid membrane and protein signals in the nano-FT-IR spectra of this mutant. Our results show, for the first time, that nano-FT-IR is an excellent means to directly probe cell wall biochemical composition in intact, single yeast cells.

ORCID iD

Kathleen M. Gough https://orcid.org/0000-0002-9581-8272

Supplemental Material

All supplemental material mentioned in the text is available in the online version of the journal.

References

1. G. Lesage, H. Bussey. "Cell Wall Assembly in *Saccharomyces cerevisiae*". Microbiol. Mol. Biol. Re 2006. 70(2): 317–343.
2. P. Orlean. "Architecture and Biosynthesis of the *Saccharomyces cerevisiae* Cell Wall". Genetics. 2012. 192(3): 775–818.
3. M. Stratford. "Another Brick in the Wall? Recent Developments Concerning the Yeast Cell Envelope". Yeast. 1994. 10(13): 1741–1752.
4. F.M. Klis, A. Boorsma, P.W.J. De Groot. "Cell Wall Construction in *Saccharomyces cerevisiae*". Yeast. 2006. 23(3): 185–202.
5. D.E. Levin. "Regulation of Cell Wall Biogenesis in *Saccharomyces cerevisiae*: The Cell Wall Integrity Signaling Pathway". Genetics. 2011. 189(4): 1145–1175.
6. M.J. Dagley, I.E. Gentle, T.H. Beilharz, F.A. Pettolino, et al. "Cell Wall Integrity is Linked to Mitochondria and Phospholipid Homeostasis in *Candida albicans* Through the Activity of the Post-Transcriptional Regulator Ccr4-Pop2". Mol. Microbiol. 2011. 79(4): 968–989.
7. J.P. Latgé. "The Cell Wall: A Carbohydrate Armour for the Fungal Cell". Mol. Microbiol. 2007. 66(2): 279–290.
8. T. Roemer, H. Bussey. "Yeast Beta-Glucan Synthesis: KRE6 Encodes a Predicted Type II Membrane Protein Required for Glucan Synthesis In Vivo and for Glucan Synthase Activity In Vitro". Proc. Natl. Acad. Sci. U.S.A. 1991. 88(24): 11295–11299.
9. T. Kurita, Y. Noda, T. Takagi, M. Osumi, K. Yoda. "Kre6 Protein Essential for Yeast Cell Wall β-1,6-Glucan Synthesis Accumulates at Sites of Polarized Growth". J. Biol. Chem. 2011. 286(9): 7429–7438.
10. T. Roemer, S. Delaney, H. Bussey. "SKN1 and KRE6 Define a Pair of Functional Homologs Encoding Putative Membrane Proteins Involved in Beta-Glucan Synthesis". Mol. Cell Biol. 1993. 13(7): 4039–4048.
11. H. Uchiyama, A. Iwai, H. Dohra, T. Ohnishi, et al. "The Effects of Gene Disruption of Kre6-Like Proteins on the Phenotype of β-Glucan-Producing *Aureobasidium pullulans*". Appl. Microbiol. Biotechnol. 2018. 102(10): 4467–4475.
12. Q. Han, N. Wang, G. Yao, C. Mu, et al. "Blocking β-1,6-Glucan Synthesis by Deleting KRE6 and SKN1 Attenuates the Virulence of *Candida albicans*". Mol. Microbiol. 2019. 111(3): 604–620.
13. Martin H., A. Dagkessamanskaia, G. Satchanska, N. Dallies, J. François. "KNR4, a Suppressor of *Saccharomyces cerevisiae* cwh Mutants, is Involved in the Transcriptional Control of Chitin Synthase Genes". Microbiology. 1999. 145(Pt. 1): 249–258.
14. H. Martin-Yken, J.M. François, D. Zerbib. "Knr4: A Disordered Hub Protein at the Heart of Fungal Cell Wall Signalling". Cell Microbiol. 2016. 18(9): 1217–1227.
15. A. Dagkessamanskaia, K.E. Azzouzi, Y. Kikuchi, T. Timmers, et al. "Knr4 N-Terminal Domain Controls its Localization and Function During Sexual Differentiation and Vegetative Growth". Yeast. 2010. 27(8): 563–574.
16. A. Dagkessamanskaia, H. Martin-Yken, F. Basmaji, P. Briza, J. Francois. "Interaction of Knr4 Protein, a Protein Involved in Cell Wall Synthesis, with Tyrosine tRNA Synthetase Encoded by TYS1 in *Saccharomyces cerevisiae*". FEMS Microbiol. Lett. 2001. 200(1): 53–58.
17. H. Martin-Yken, T. Bedekovic, A.C. Brand, M.L. Richard, et al. "A Conserved Fungal Hub Protein Involved in Adhesion and Drug Resistance in the Human Pathogen *Candida albicans*". Cell Surf. 2018. 4(October): 10–19.
18. J.E. Nett, H. Sanchez, M.T. Cain, K.M. Ross, D.R. Andes. "Interface of *Candida albicans* Biofilm Matrix-Associated Drug Resistance and Cell Wall Integrity Regulation". Eukaryot Cell. 2011. 10(12): 1660–1669.
19. G. Bakir, B.E. Girouard, R.W. Johns, C.R.-J. Findlay, et al. "Ultrastructural and SINS Analysis of the Cell Wall Integrity Response of: *Aspergillus nidulans* to the Absence of Galactofuranose". Analyst. 2019. 144(3): 928–934.
20. E. Burattini, M. Cavagna, R. Dell'Anna, F. Malvezzi Campeggi, et al. "A FTIR Microspectroscopy Study of Autolysis in Cells of the Wine Yeast *Saccharomyces cerevisiae*". Vib. Spectrosc. 2008. 47(2): 139–147.
21. M. Cavagna, R. Dell'Anna, F. Monti, F. Rossi, S. Torriani. "Use of ATR-FTIR Microspectroscopy to Monitor Autolysis of *Saccharomyces cerevisiae* Cells in a Base Wine". J. Agric. Food Chem. 2010. 58(1): 39–45.
22. J. Šandula, G. Kogan, M. Kačuráková, E. Machová. "Microbial (1→3)-β-D-Glucans, Their Preparation, Physico-Chemical Characterization, and Immunomodulatory Activity". Carbohydr. Polym. 1999. 38(3): 247–253.
23. Bechtel H.A., E.A. Muller, R.L. Olmon, M.C. Martin, M. B. Raschke. "Ultrabroadband Infrared Nanospectroscopic Imaging". Proc. Natl. Acad. Sci. U.S.A. 2014. 111(20): 7191–7196.
24. D. Nečas, P. Klapetek. "Gwyddion: An Open-Source Software for SPM Data Analysis". Cent. Eur. J. Phys. 2012. 10(1): 181–188.
25. F. Huth, A. Govyadinov, S. Amarie, W. Nuansing, et al. "Nano-FTIR Absorption Spectroscopy of Molecular Fingerprints at 20 nm Spatial Resolution". Nano Lett. 2012. 12(8): 3973–3978.

26. S. Mastel, A.A. Govyadinov, T.V.A.G. De Oliveira, I. Amenabar, R. Hillenbrand. "Nanoscale-Resolved Chemical Identification of Thin Organic Films Using Infrared Near-Field Spectroscopy and Standard Fourier Transform Infrared References". Appl. Phys. Lett. 2015. 106(2): 1–6.

27. H.A. Bechtel, S.C. Johnson, O. Khatib, E.A. Muller, M.B. Raschke. "Synchrotron Infrared Nano-Spectroscopy and Imaging". Surf. Sci. Rep. 2020. 75(3): 100493.

28. Z. Hromádková, A. Ebringerová, V. Sasinková, J. Šandula, et al. "Influence of the Drying Method on the Physical Properties and Immunomodulatory Activity of the Particulate (1 → 3)-β-D-Glucan from Saccharomyces cerevisiae". Carbohydr. Polym. 2003. 51(1): 9–15.

29. M. Mehranian, R.F. Pourabad, N.S. Bashir, S. Taieban. "Physicochemical Characterization of Chitin from the Mediterranean Flour Moth, Ephestia Kuehniella Zeller (Lepidoptera: Pyralidae)". J. Macromol. Sci., Part A: Pure Appl. Chem. 2017. 54(10): 720–726.

30. V. Zechner-Krpan, V. Petravić-Tominac, I. Gospodarić, L. Sajli, et al. "Characterization of β-Glucans Isolated from Brewer's Yeast and Dried by Different Methods". Food Technol. Biotechnol. 2010. 48(2): 189–197.

31. P. Bassan, A. Kohler, H. Martens, J. Lee, et al. "Resonant Mie Scattering (RMieS) Correction of Infrared Spectra from Highly Scattering Biological Samples". Analyst. 2010. 135(2): 268–277.

32. G. Mie. "Beiträge zur Optik Trüber Medien, Speziell Kolloidaler Metallösungen". Ann. Phys. 1908. 330(3): 377–445.

33. B. Mohlenhoff, M. Romeo, M. Diem, B.R. Wood. "Mie-Type Scattering and Non-Beer–Lambert Absorption Behavior of Human Cells in Infrared Microspectroscopy". Biophys. J. 2005. 88(5): 3635–3640.

34. T.H. Nguyen, G.H. Fleet, P.L. Rogers. "Composition of the Cell Walls of Several Yeast Species". Appl. Microbiol. Biotechnol. 1998. 50(2): 206–212.

35. A. Galichet, G.D. Sockalingum, A. Belarbi, M. Manfait. "FTIR Spectroscopic Analysis of Saccharomyces cerevisiae Cell Walls: Study of an Anomalous Strain Exhibiting a Pink-Colored Cell Phenotype". FEMS Microbiol. Lett. 2001. 197(2): 179–186.

36. A.J. Michell, G. Scurfield. "An Assessment of Infrared Spectra as Indicators of Fungal Cell Wall Composition". Aust. J. Biol. Sci. 1970. 23(2): 345.

37. J.C. Kapteyn, P. Van Egmond, E. Sievi, H. Van Den Ende, et al. "The Contribution of the O-Glycosylated Protein Pir2p/Hsp150 to the Construction of the Yeast Cell Wall in Wild-Type Cells and β1,6-Glucan-Deficient Mutants". Mol. Microbiol. 1999. 31(6): 1835–1844.

38. F.M. Klis, P. Mol, K. Hellingwerf, S. Brul. "Dynamics of Cell Wall Structure in Saccharomyces cerevisiae". FEMS Microbiol. Rev. 2002. 26(3): 239–256.

39. E. Dague, R. Bitar, H. Ranchon, F. Durand, et al. "An Atomic Force Microscopy Analysis of Yeast Mutants Defective in Cell Wall Architecture". Yeast. 2010. 27(8): 673–684.

40. Findlay C.R., R. Wiens, M. Rak, J. Sedlmair, et al. "Rapid Biodiagnostic Ex Vivo Imaging at 1 μm Pixel Resolution with Thermal Source FTIR FPA". Analyst. 2015. 140(7): 2493–2503. 10.1039/C4AN01982B

41. Saulou C., F. Jamme, C. Maranges, I. Fourquaux, et al. "Synchrotron FTIR Microspectroscopy of the Yeast Saccharomyces cerevisiae After Exposure to Plasma-Deposited Nanosilver-Containing Coating". Anal. Bioanal. Chem. 2010. 396(4): 1441–1450.

42. S. Kaminskyj, K. Jilkine, A. Szeghalmi, K. Gough. "High Spatial Resolution Analysis of Fungal Cell Biochemistry: Bridging the Analytical Gap Using Synchrotron FTIR Spectromicroscopy". FEMS Microbiol. Lett. 2008. 284(1): 1–8.

43. A. Szeghalmi, S. Kaminskyj, K.M. Gough. "A Synchrotron FTIR Microspectroscopy Investigation of Fungal Hyphae Grown Under Optimal and Stressed Conditions". Anal. Bioanal. Chem. 2007. 387(5): 1779–1789.

44. V. Dupres, Y.F. Dufrêne, J.J. Heinisch. "Measuring Cell Wall Thickness in Living Yeast Cells Using Single Molecular Rulers". ACS Nano. 2010. 4(9): 5498–5504.

45. Z. Hong, P. Mann, N.H. Brown, L.E. Tran, et al. "Cloning and Characterization of KNR4, a Yeast Gene Involved in (1,3)-β-Glucan Synthesis". Mol. Cell Biol. 1994. 14(2): 1017–1025.